Electrochemical Study of DPPH Radical Scavenging for Evaluating the Antioxidant Capacity of Carbon Nanodots

By: Wendi Zhang, Zheng Zeng, and Jianjun Wei

W. Zhang, Z. Zeng, J. Wei, Electrochemical Study of DPPH Radical Scavenging for Evaluating the Antioxidant Capacity of Carbon Nanodots, *Journal of Physical Chemistry C*. **2017**, 121 (34), 18635–18642. DOI: 10.1021/acs.jpcc.7b05353.

Abstract:

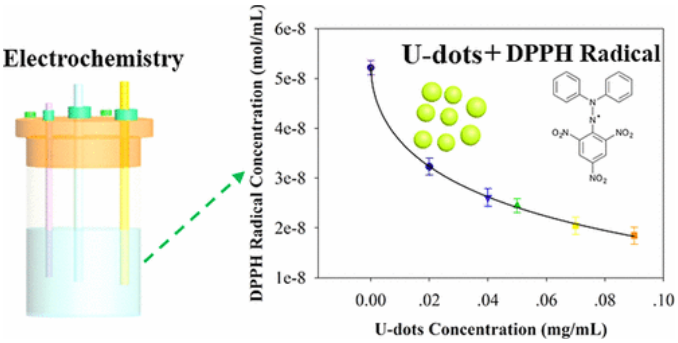

Carbon nanodots (CNDs) have become one of the potential candidates for antioxidants due to their excellent luminescence, biocompatibility, and lower cytotoxicity. While CNDs have experienced some research on radical scavenging activity via UV–vis spectroscopy, the relationship between reserved 2,2-diphenyl-1-picrylhydrazyl radical (DPPH$^{\bullet}$) concentration and CNDs' incubation concentration remains unclear. This work describes an electrochemical study on the changes of redox peaks of the oxidation of DPPH$^{\bullet}$ at gold electrodes with addition of different concentrations of a type of microwave-synthesized CND (U-dots). The result is consistent with a UV–vis absorption dose-dependent study used to quantify the antioxidation activities. Combined with standard heterogeneous electron-transfer rate constant analysis, electrochemical study gives a coupled hydrogen atom transfer (HAT) mechanism for DPPH$^{\bullet}$ scavenging by the U-dots. This work provides a new perspective on the antioxidative study of the U-dots, which may aid their development for practical use in biomedicine.

Keywords: carbon nanodots (CNDs) | DPPH radical | electrochemistry | U-dots | antioxidation activity

Article:

Introduction

Carbon nanodots (CNDs) have been prepared in several different ways, including chemical ablation, electrochemical carbonization, laser ablation, hydrothermal/solvothermal treatment, and microwave irradiation, and they have found applications in biomedicine, chemical sensing, and photoelectric devices.[1-4] Their physicochemical properties of good solubility, low toxicity, and biocompatibility and their optoelectronic properties of strong fluorescence, phosphorescence, chemiluminescence, and photoinduced electron transfer make them particularly desirable.[5-8] Reportedly, CNDs could act as antioxidants and prooxidants due to their roles as electron donors or electron acceptors.[9] Xu et al. studied the antioxidative ability of CNDs at the cellular level, which showed good potential for applying CNDs to protect cells against oxidative stress.[10] Das et al. used microwave-synthesized CNDs to scavenge reactive oxygen species like hydroxyl radicals and superoxides in a cellular microenvironment.[11]

The nitrogen-centered 2,2-diphenyl-1-picrylhydrazyl radical (DPPH$^{\bullet}$)-based assay has been one of the most commonly employed species to evaluate the antioxidant activity[12] because it can change its color from deep violet to light yellow in a dark environment when in contact with antioxidants due to the DPPH$^{\bullet}$ being converted into a stable DPPH–H complex, which could be calculated by comparing the absorbance at 517 nm against the blank by ultraviolet–visible (UV–vis) spectroscopy.[13] Although CNDs have experienced some research on their antioxidation properties via the DPPH$^{\bullet}$-based assay, UV–vis spectroscopy has been the only tool to test the absorbance change under different incubation concentrations of CNDs. A poor understanding about the relationship between the reserved DPPH$^{\bullet}$ concentration and CND incubation concentration and underlying antioxidation reactions limits their potential applications in biology fields, especially in biomedicine.

Electrochemistry could be another powerful tool to determine the concentration relationship via the cyclic voltammetry method because redox peak currents and peak potentials are related to the parameters of bulk diffusion species, such as the bulk concentration, diffusion coefficient, number of electrons involved, and heterogeneous electron-transfer rate constant.[14-16] This work reports an electrochemical study to investigate the change of redox peaks of the DPPH$^{\bullet}$–gold electrode system incubated with different concentrations of CNDs synthesized from citric acid and urea (named U-dots). Here, water-soluble U-dots were synthesized by a simple one-step microwave route and were characterized by transmission electron microscopy (TEM), atomic force microscope (AFM), X-ray photoelectron spectroscopy (XPS), Fourier transform infrared spectroscopy (FTIR), Raman spectroscopy, X-ray powder diffraction (XRD), UV–vis spectroscopy, fluorescence spectroscopy, and quantum yield measurements. An analytical model was used to examine the reserved DPPH$^{\bullet}$ concentration and standard heterogeneous electron-transfer rate constant changes in the DPPH$^{\bullet}$–gold electrode system incubated by different concentrations of U-dots. The results were compared with antioxidation activity changes measured by absorbance at 517 nm via UV–vis spectroscopy, which further activates the mechanism study of DPPH$^{\bullet}$ scavenging by the U-dots.

Experimental Section

Synthesis of U-dots. Microwave-assisted synthesis of CNDs was performed using citric acid and urea as precursors.[17] Briefly, 1.0 g of urea (99.5%, Aldrich) and 1.0 g of citric acid (99%, ACROS Organics) were simultaneously added to 1.0 mL of deionized water to form a

homogeneous solution, and then, the solution was heated in a microwave synthesizer (CEM Corp 908005 Microwave Reactor Discovery System) at a power of 300 W for 18 min. After cooling, the aqueous reaction mixture was purified using a centrifuge (Solvall Legend XFR Floor Model Centrifuge) at 3500 r/min for 20 min to remove large and aggregated particles. The dark-brown solution was further purified by deionized water using a dialysis membrane (Scientific Fisher) with a molecular weight cutoff of 1000 Da for 24 h. To obtain the solid sample, the resultant solution was finally dried with a freeze-dryer (Labconco Free Zone 6 Freeze-Dryer) for 24 h. We named this type of CNDs U-dots.

U-dots Characterization. Transmission electron microscopy (TEM, Carl Zeiss Libra 120 Plus) of U-dots on a grid substrate and atomic force microscope (AFM, Agilent Technologies 5600 LS Series) of U-dots on a mica substrate in contact mode were used to study the size of the CNDs. XRD (Agilent Technologies Oxford Gemini), FTIR (Varian 670), XPS (Thermo Fisher ESCALAB 250 Xi), and Raman spectroscopy (Horiba XploRA One Raman Confocal Microscope System) were employed to analyze the elemental composition and chemical structure of the U-dots. UV–vis spectroscopy (Varian Cary 6000i) of different concentrations of U-dots and fluorescence spectroscopy (Varian Cary Eclipse) (at 0.05 mg/mL of U-dots) were used to investigate the absorbance and fluorescence properties of U-dots, respectively.

UV–Vis Study of Antioxidation Activity. The antioxidation activity of U-dots for DPPH$^{\bullet}$ (95%, Alfa Aesar) was evaluated by monitoring the absorbance change at 517 nm via UV–vis spectroscopy.[18] For each measurement, the DPPH$^{\bullet}$ was prepared with a final concentration of 0.02 mg/mL (52 nmol/mL) in absolute methanol incubated in different concentrations of U-dots in a dark environment for 1.5 h.

Electrochemistry Study. Electrochemical measurements were performed using a three-electrode electrochemical cell with a gold working electrode (Fisher Scientific), a Ag/AgCl reference electrode (Fisher Scientific), and a platinum counter electrode (Fisher Scientific) in a 5.0 mL methanolic phosphate buffer with pH 7.2 (Fisher Scientific pH 2100), a 1:1 mixture of absolute methanol (Fisher Scientific) and a phosphate buffer (pH 7.0, Life Tech) solution containing 0.02 mg/mL (52 nmol/mL) DPPH$^{\bullet}$ incubated by different concentrations of U-dots for 1.5 h under a dark environment. Cyclic voltammetry of the samples was run at different scan rates at room temperature.

Results and Discussion

U-dots Synthesis and Characterization. An easy, economic, one-step microwave route was used to synthesize U-dots from citric acid and urea.[17] TEM (Figures 1A and S1) and AFM (Figures 1B and S2) studies indicate that the U-dots are well dispersed and have an average size of 2.4 ± 0.3 nm. The main diffraction peak in the XRD spectrum (Figure 1C) appears at 22.9° with a full width at half-maximum (fwhm) of about 3.7°, corresponding to an interlayer distance of 0.39 nm between the planar carbon-based sheets for the disordered graphite structure region,[19] which is further supported by the Raman spectra of the U-dots (Figure 1C inset). The D bands at 1338 cm^{-1} (sp^3-hybridized) and G bands at 1568 cm^{-1} (sp^2-hybridized) present an intensity ratio I_D/I_G of about 1.04.[20, 21] FTIR spectra of the U-dots (Figure 1D) display broad bands at 3100–3400 cm^{-1} that are assigned to ν(O–H) and ν(N–H). The IR transitions at 754,

1183, 1397, and 1576 cm^{-1} are assigned to ν(C–C), ν(C–O), ν(C═C), and ν(C═O), respectively,[22] which are also supported by XPS data (Figure 1E) of the U-dots. The XPS data demonstrate four components: C═C (39.9%, 284.2 eV), C–C (8.7%, 284.7 eV), C═O (42.1%, 287.6 eV), and C–O (7.9%, 286.2 eV). The presence of functionalities (−COOH and $-NH_3$) (Figures 1E, S3, and S4) helps explain the hydrophilicity and stability of the CNDs in aqueous media.[23-25] From the characterization results, the structures of the as-prepared U-dots are spherical with an average size of 2.4 ± 0.3 nm, and they are composed of a disorder graphite structure with surrounding amorphous carbon frames and different functional groups on the surfaces.[26]

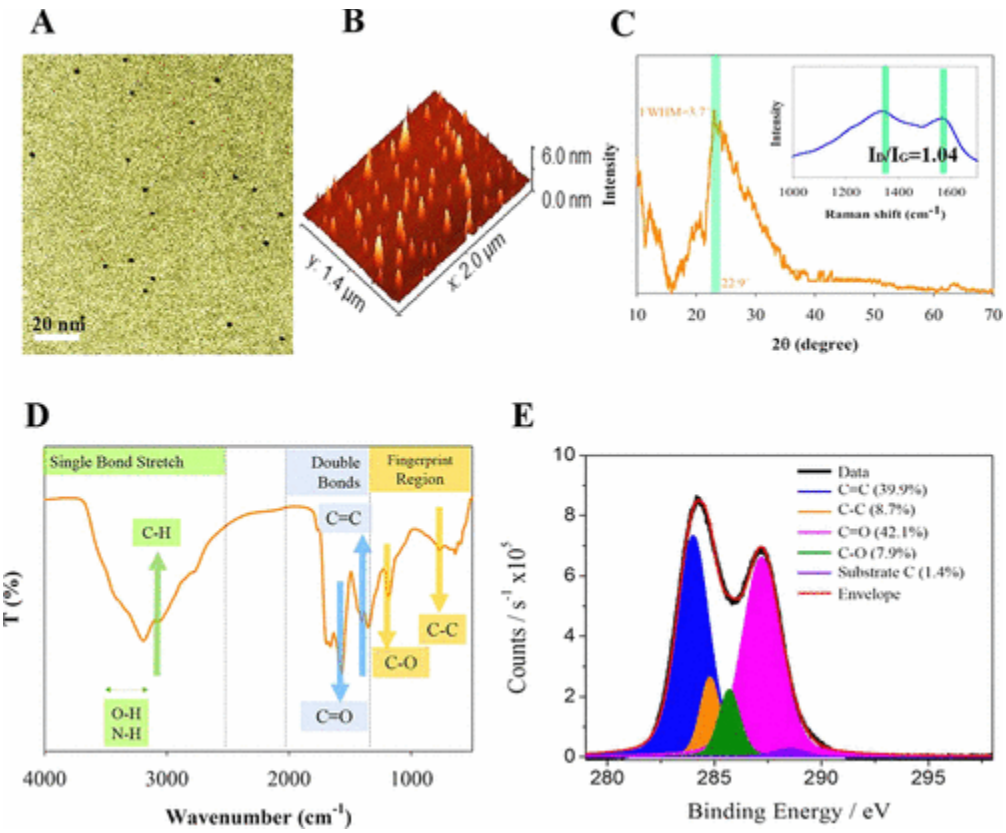

Figure 1. U-dots are characterized using different techniques: transmission electron microscopy (A), atomic force microscope (B), X-ray diffraction data with the Raman spectrum inset (C), Fourier transform infrared spectrum (D), and an X-ray photoelectron spectrum (C signal) (E).

Figure 2A shows that there is no obvious absorption feature found above 600 nm. The main peak at 337 nm comes from the n–π* transition of the C═O bond. Figure 2B shows the fluorescence emission spectra of U-dots in deionized water at seven different excitation wavelengths (λ_{ex} = 330, 360, 390, 420, 450, 480, and 510 nm). The maximum emission intensity occurs with 360 nm excitation and has a peak emission at 447 nm. The apparent red shift in the photoluminescence spectra with changing excitation wavelength indicates that U-dots can act as blue/green fluorophores in imaging applications, which is in agreement with other reports.[27-29] Furthermore, the quantum yield of U-dots was investigated according to established methods.[30] Quinine sulfate (quantum yield of 0.54 at 360 nm) dissolved in 0.1 M H_2SO_4 (refractive index = 1.33) was chosen as the reference. The absorbance and photoluminescence intensity

measurements via the UV–vis spectrometer and photoluminescence spectrometer give a quantum yield of about 0.091 for the as-prepared U-dots.

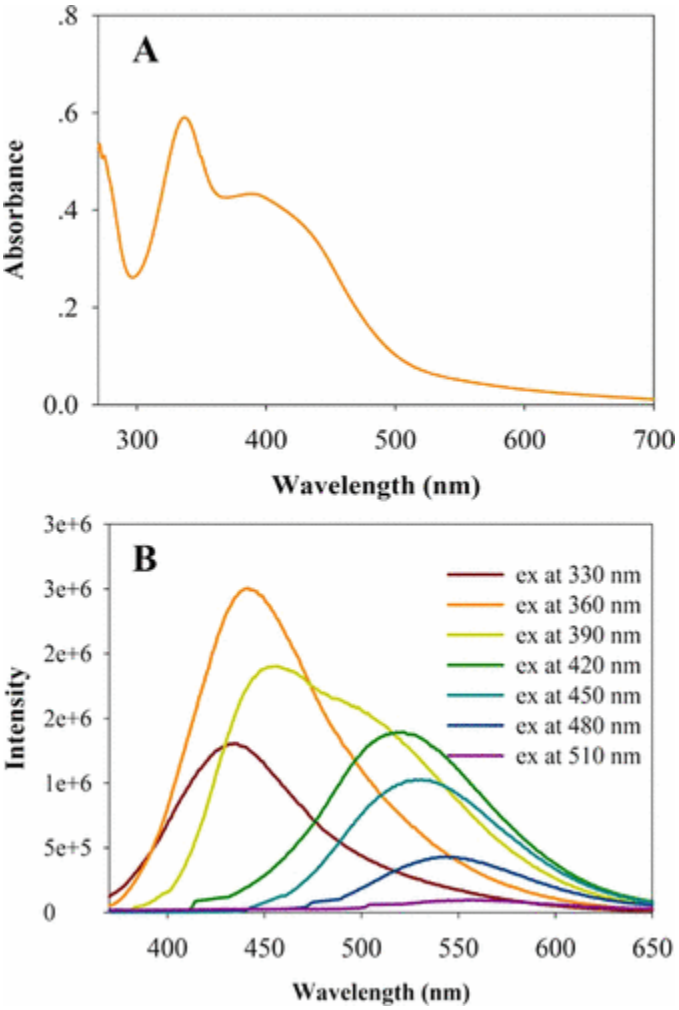

Figure 2. (A) UV–vis absorption spectrum of U-dots. (B) Fluorescence emission spectra of U-dots in deionized water.

UV–Vis Study of Antioxidation Activity of U-dots. The antioxidation activity was evaluated by using the DPPH•-based array via UV–vis spectroscopy. DPPH• is known as a stable free radical that resulted from delocalization of the spare electron, which shows a deep violet color in methanol solution.[31] However, upon addition of different concentrations of U-dots, the absorbance of DPPH• methanol solutions at 517 nm decreases, as shown in Figure 3A, and its color changes from deep violet to pale yellow. According to the following equation

$$\text{antioxidation activity (\%)} = \frac{A_0 - A_c}{A_0} \times 100 \quad (1)$$

where A_0 and A_c are the absorbance of DPPH• at 517 nm in the absence and presence of U-dots, respectively, the antioxidation activity is obtained to be about 23.3, 52.4, 73.0, 82.4, and 87.3% at U-dot concentrations of 0.02, 0.04, 0.05, 0.07, and 0.09 mg/mL, respectively. A minimum of

three trials of each concentration were measured, and the DPPH•–U-dots incubation reached its steady state after 1.5 h and was highly reproducible. The error bars are too minimal to see in Figure 3B. A subsequent increase in the antioxidant activity presents a dose-dependent manner, and the antioxidant activity is observed to have a plateau region at higher concentrations of U-dots (Figure 3B).

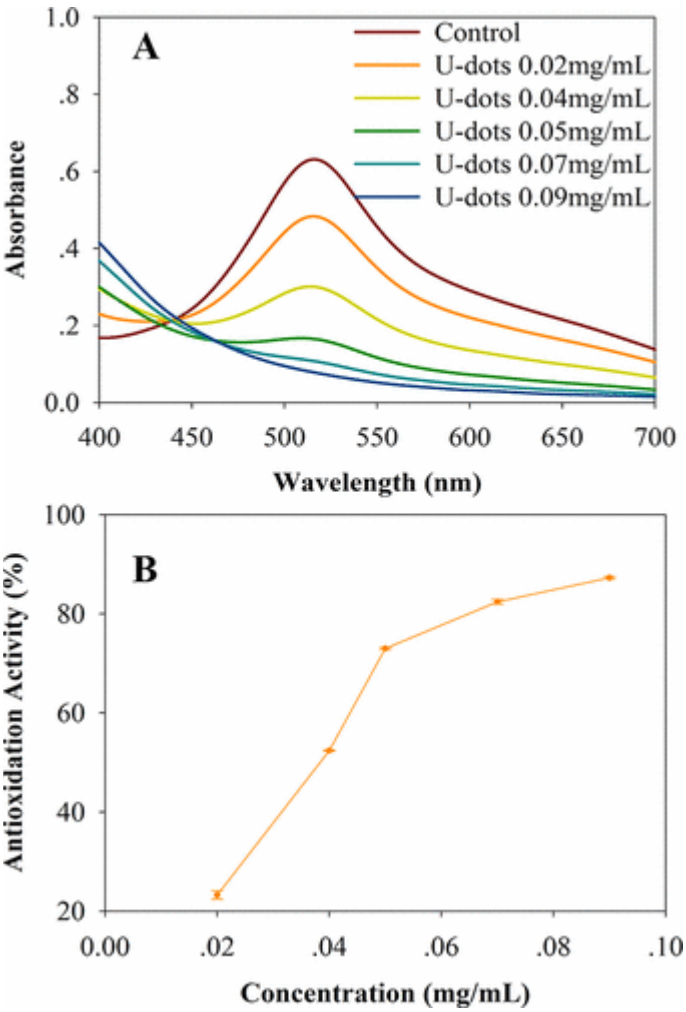

Figure 3. (A) Absorption spectra of 0.02 mg/mL DPPH• methanol solutions with increasing U-dots concentration from 0 to 0.09 mg/mL measured after incubation for 1.5 h under a dark environment. (B) Calculated antioxidation activity versus U-dots concentration (very reproducible, and the error bar is very small, as Table 1 shows).

Electrochemical Study of DPPH• Scavenging Activity of U-dots. The electrode reactions of DPPH• are of interest due to free radicals frequently being intermediates and products of electrode reactions, following reversible, one-electron reactions[32]

$$\text{Oxidation: } DPPH^{\bullet} - e \rightarrow DPPH^{+} \quad (2)$$

$$\text{Reduction: } DPPH^{\bullet} + e \rightarrow DPPH^{-} \quad (3)$$

In general, the peaks of both redox couples (oxidation: α/α′ couple; reduction: β/β′ couple) could be observed in most of the solutions during the cyclic voltammetry. However, in a 5.0 mL methanolic phosphate buffer solution using a gold working electrode, the β/β′ couple was found to be irreversible (Figure S5), suggesting that the reduction product is particularly unstable in this solution.[33] Hence, for the purpose of the electrochemical electron-transfer study in this work, we focus on the α/α′ redox reaction. The cyclic voltammograms of DPPH$^{\bullet}$ incubated by different concentrations of U-dots at different scan rates show a pair of redox peaks (Figure 4). The cathodic peak resulted from the electrochemical reduction of DPPH$^{\bullet}$ and the decrease in the intensity of the anodic and cathodic peaks present (Figures 4 and 5A) with increasing concentration of U-dots. Because no measurable redox peaks are shown for 0.05 mg/mL U-dots in a 5.0 mL methanolic phosphate buffer (Figure S6) or the stable cyclic voltammograms of 0.01 mg/mL DPPH$^{\bullet}$ in a 5.0 mL methanolic phosphate buffer (but lower peak currents compared to 0.02 mg/mL DPPH$^{\bullet}$) without U-dot incubation as a control (Figure S7), the decrease in the intensity of the anodic and cathodic peaks for DPPH$^{\bullet}$ incubated by different concentrations of U-dots is due to the decrease in the concentration of DPPH$^{\bullet}$. A similar method and results have been reported for the scavenging of DPPH$^{\bullet}$ by using Trolox in ethanolic phosphate buffer and flavonoids in an aprotic medium.[34, 35] The fwhm of the reduction peak gives a value of about 116 mV, corresponding to a one-electron-transfer redox reaction (Figure 5A). In addition, the peak current, i_p (A), is measured as a function of the square root of the voltage scan rate at different concentrations of U-dots and is found to exhibit a linear dependence (Figure 5B). The dependence of the peak current position on the square root of the voltage scan rate for the DPPH$^{\bullet}$ without U-dot incubation can be first used to characterize the diffusion coefficient (D_0, cm^2/s) of DPPH$^{\bullet}$ through the Randles–Sevcik equation[36, 37]

$$i_p = (2.69 \times 10^5) n^{3/2} A C D_0^{1/2} \nu^{1/2} \tag{4}$$

where n is the number of electrons exchanged, A is the active surface area of the gold electrode (0.043 cm^2), C is the concentration of the DPPH$^{\bullet}$ (mol/mL), and ν is the voltage scan rate (V/s). The diffusion coefficient of DPPH$^{\bullet}$ is found to be about 1.24×10^{-5} cm^2/s. By using eq 4, this value can then be coupled with plots of the dependence at different concentrations of U-dots (Figure 5B) to extract the concentration of the DPPH$^{\bullet}$ values for different systems (Figure 5C). The reserved DPPH$^{\bullet}$ concentration is obtained to be about 32.3, 26.1, 24.5, 20.4, and 18.5 nmol/mL at U-dot concentrations of 0.02, 0.04, 0.05, 0.07, and 0.09 mg/mL (Table 1) with radical scavenging activity of about 38.1, 49.9, 53.1, 60.8, and 64.6%, respectively (Figure 5C inset) according to eq 5.

$$\text{Scavenging activity (\%)} = \frac{C_0 - C_c}{C_0} \times 100 \tag{5}$$

where C_0 and C_c are the concentration of DPPH$^{\bullet}$ in the absence and presence of U-dots, respectively. The data are then best fitted by the following equation

$$C_{\text{DPPH}^{\bullet}} = \frac{0.0277}{1 + \left(\frac{C_{\text{U-dots}}}{-0.1019}\right)^{0.5728}} - 0.0071 \tag{6}$$

where $C_{DPPH^{\bullet}}$ (mg/mL) and $C_{U\text{-}dots}$ (mg/mL) are the concentrations of reserved DPPH$^{\bullet}$ and U-dot addition, respectively, which have the same trend as the antioxidation activity shown in Figure 3. Furthermore, the ratio of the anodic peak current to the cathodic one closes to 1 for each scan rate, suggesting that a heterogeneous electron transfer is present. Also, the slope of the linearization decreases with the increase of U-dot concentrations, indicating that U-dots weaken the electron transfer in the DPPH$^{\bullet}$–gold electrode system.

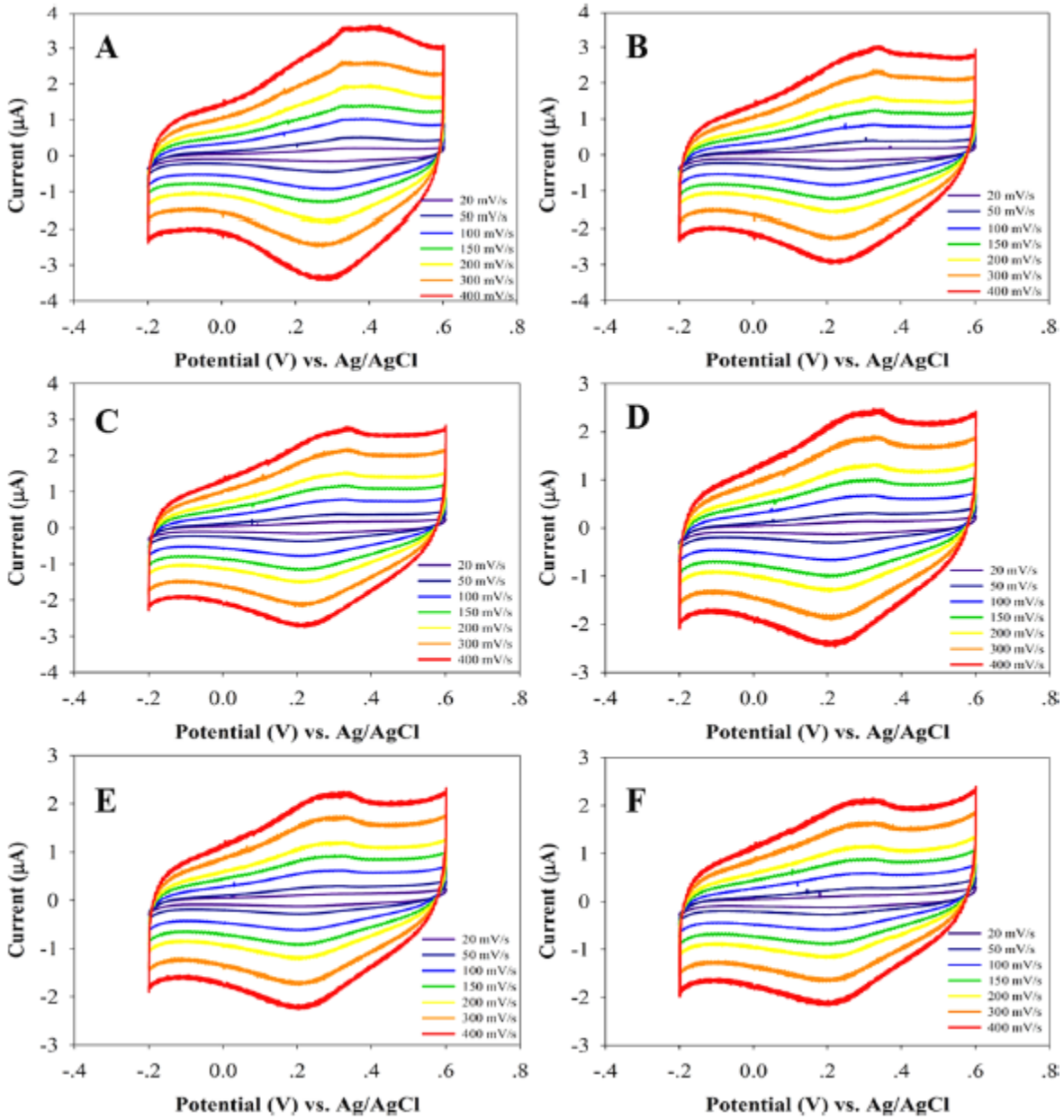

Figure 4. Cyclic voltammograms for the DPPH$^{\bullet}$–gold electrode system incubated by 0.00 (A), 0.02 (B), 0.04 (C), 0.05 (D), 0.07 (E), and 0.09 mg/mL (F) U-dots for 1.5 h under a dark environment at 20, 50, 100, 150, 200, 300, and 400 mV/s scan rates.

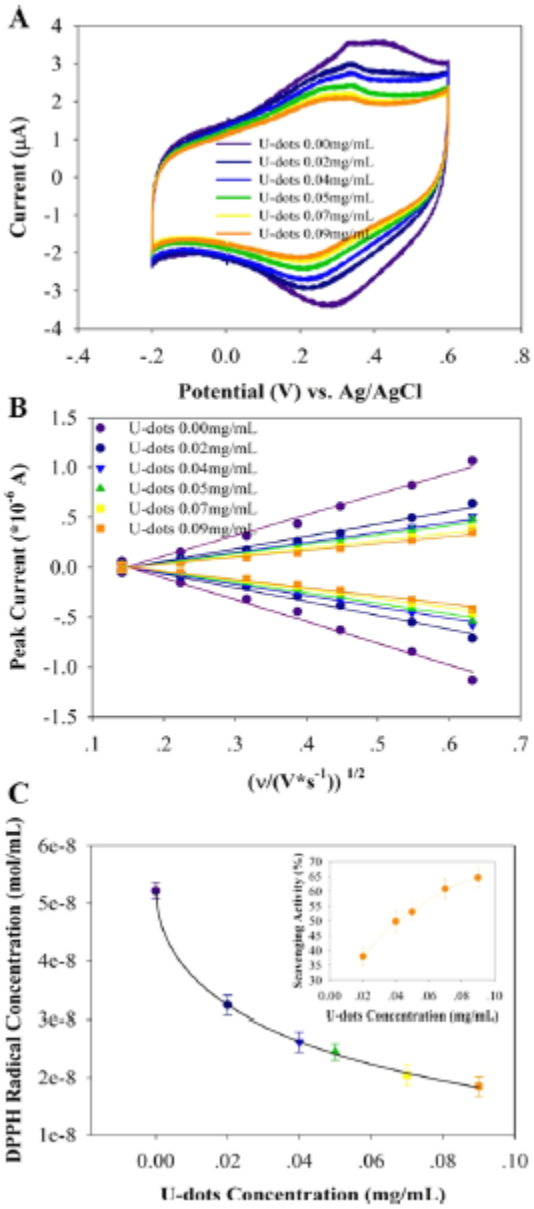

Figure 5. (A) Cyclic voltammograms for the DPPH•–gold electrode system incubated by different concentrations of U-dots at a scan rate of 400 mV/s. (B) Representative plot of the linear dependence of the peak current on the voltage scan rate incubated by different concentrations of U-dots (using the data of Figure 4). (C) Reserved DPPH• concentration estimation with the best fit after incubation with different concentrations of U-dots for 1.5 h under a dark environment (error bars indicate the standard deviation for three trials, as Table 1 shows). (Inset) Calculated scavenging activity versus U-dot concentration.

Table 1. Antioxidation Activities of Different Concentrations of U-dots and the Reserved DPPH$^{\bullet}$ Concentration and Standard Heterogeneous Electron-Transfer Rate Constant Data for The DPPH$^{\bullet}$–Gold Electrode System Incubated by U-dots

U-dots concentration (mg/mL)	antioxidation activity (%)	DPPH$^{\bullet}$concentration (nmol/mL)	k^0 (cm/s)
0.00	0	52.2 ± 1.4	0.0093 ± 0.0015
0.02	23.30 ± 0.08	32.3 ± 1.7	0.0061 ± 0.0009
0.04	52.38 ± 0.01	26.1 ± 1.8	0.0058 ± 0.0007
0.05	72.98 ± 0.02	24.5 ± 1.4	0.0055 ± 0.0005
0.07	82.42 ± 0.05	20.4 ± 1.7	0.0049 ± 0.0003
0.09	87.26 ± 0.02	18.5 ± 1.7	0.0046 ± 0.0002

The dependence of the redox peak's position on the voltage scan rate can be used to characterize the electron-transfer rate constant. The electron-transfer reaction can be written as eq 7 with the oxidation electron-transfer rate of k_{ox} from DPPH$^{\bullet}$ to DPPH^{+} and the reversed reduction electron-transfer rate of k_{red} from DPPH^{+} to DPPH$^{\bullet}$

$$\mathrm{Red} - \mathrm{e} \underset{k_{\mathrm{red}}}{\overset{k_{\mathrm{ox}}}{\rightleftarrows}} \mathrm{Ox} \tag{7}$$

where Red and Ox represent DPPH$^{\bullet}$ and DPPH^{+}, respectively. The Gibbs free energy of this reaction can be easily changed by the applied external potential; therefore, the electron-transfer rate k_{ox} or k_{red} is also subjected to the potential. In the case of the equilibrium state, $k_{ox} = k_{red} = k^0$ is the standard heterogeneous rate constant given by[38]

$$k^0 = 2.18\left(\frac{\alpha D_0 nF\nu}{RT}\right)^{1/2} \exp\left[\frac{-\alpha^2 nF\left(E_{\mathrm{pa}} - E_{\mathrm{pc}}\right)}{RT}\right] \tag{8}$$

where α is the transfer coefficient, D_0 is the diffusion coefficient (cm^2/s), F is Faraday's constant, R is the gas constant, T is temperature in Kelvin, and E_{pa} and E_{pc} are the anodic and cathodic peak potentials, respectively. These calculations can then be compared to plots of the experimental Faradaic peak potential shift from apparent formal potential versus voltage scan rates (Figure 6A) to extract the k^0 values for different systems (Figure 6B). In the absence of U-dots, the standard heterogeneous electron-transfer rate constant (k^0) for the DPPH$^{\bullet}$–gold electrode system is calculated to be ∼0.0093 cm/s. After DPPH$^{\bullet}$ incubation by U-dots for 1.5 h under a dark environment, k^0 is found to be about 0.0061, 0.0058, 0.0055, 0.0049, and 0.0046 cm/s at U-dot concentrations of 0.02, 0.04, 0.05, 0.07, and 0.09 mg/mL (Table 1), which decreased by about 34.9, 37.5, 40.6, 47.0, and 50.5%, respectively (Figure 6B inset), compared to that without U-dot incubation. The standard heterogeneous electron-transfer rate constant decrease could be the result of two phenomena; the first is a decrease in the mass transfer due to a low concentration gradient according to Fick's law that resulted from DPPH$^{\bullet}$ converted into a stable DPPH–H complex, as mentioned above (Figure 5 and ∼0.0063 cm/s for 0.01 mg/mL DPPH$^{\bullet}$ in Figure S7),[39] and the second is an increase of the diffusive mass and friction in the solution due to the DPPH$^{\bullet}$–U-dots complex formation along the DPPH$^{\bullet}$ diffusion direction; this suggests a lower reserved concentration of DPPH$^{\bullet}$ due to the U-dot incubation, which indirectly proves the DPPH$^{\bullet}$ scavenging activity of U-dots.

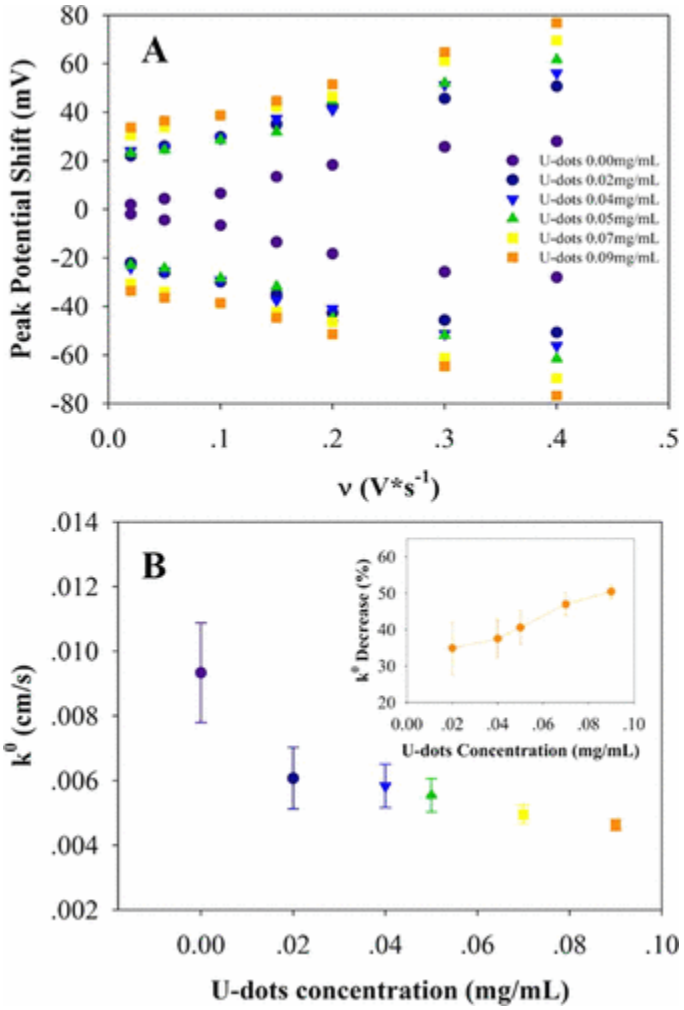

Figure 6. (A) Dependence of the peak potential shift on the scan rate shown for the DPPH•–gold electrode system incubated by different concentrations of U-dots (using the data of Figure 4). (B) Plot of k^0 versus different concentrations of U-dots (error bars indicate the standard deviation for three trials, as Table 1 shows). (Inset) k^0 decrease versus U-dot concentration.

The entire picture described above leads to an understanding of how different concentrations of U-dot incubation affect the reserved concentration of DPPH• and electron transfer of the DPPH•–gold electrode system. As shown in Figure 7, in the absence of U-dot incubation, this general electrochemical process shows that the observed redox peak currents (α/α′ couple as highlighted) are dependent upon mass transport of DPPH• with a diffusion coefficient of about 1.24×10^{-5} cm^2/s, which occurs in series with a standard heterogeneous electron-transfer rate constant of 0.0093 ± 0.0015 cm/s. However, in the presence of U-dot incubation, a proton is taken up from the U-dots and the DPPH• is changed into DPPH–H (a neutral species) via a hydrogen atom transfer (HAT) mechanism because U-dots have surface-active groups like the carboxyl group (−COOH) acting as proton donors.[40] Note that the electron cloud density between the hydrogen and oxygen in the carboxyl group is small due to the carboxyl group having an electron-withdrawing “carbonyl”, and −COO– is highly stable after deprotonation of the carboxyl group. Therefore, together with standard heterogeneous electron-transfer rate constant analysis, higher

concentrations of U-dot incubation result in lower reserved concentrations of DPPH• to conduct redox reaction, as shown in eq 6 for the relationship between reserved DPPH• concentration and U-dot incubation concentration, which highly supports the antioxidation activity test by UV–vis spectroscopy.

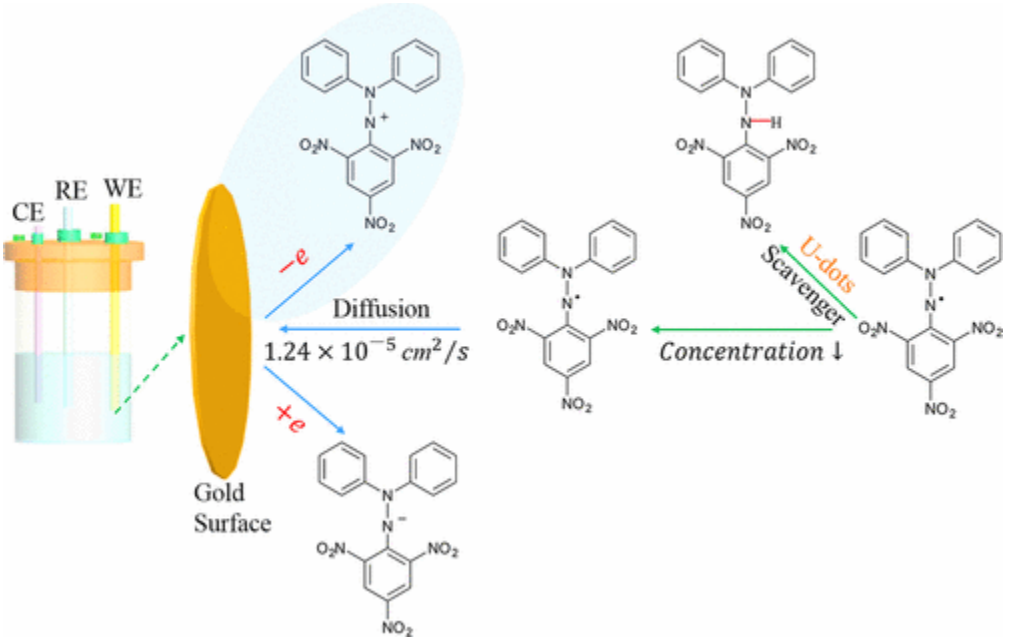

Figure 7. Mechanistic insight for the electrochemical studies of the oxidation of DPPH• during radical scavenging by the U-dot incubation.

Conclusions

This work demonstrates a new strategy for exploring the antioxidation activity of microwave-synthesized CNDs (U-dots) by investigating the reserved DPPH• concentration and standard heterogeneous electron-transfer rate constant changes in the DPPH•–gold electrode system with U-dots incubation. The relationship between the reserved DPPH• concentration and CND incubation concentration obtained from the electrochemical studies supports the UV–vis absorption dose-dependent results via a HAT mechanism, which should aid the development of this type of CNDs for practical use in biomedicine.

Supporting Information

The Supporting Information is available free of charge on the ACS Publications website at DOI: 10.1021/acs.jpcc.7b05353.

Author Contributions

W.Z. and Z.Z. contributed equally to this work. The manuscript was written with contributions by all authors. All authors have approved the final version of the manuscript.

Funding Information

This work is partially supported by National Institutes of Health under Award Number R15HL129212 and NC State fund through the Joint School of Nanoscience and Nanoengineering (JSNN). The authors declare no competing financial interest.

Acknowledgment
The authors would like to thank Dr. Brain Bloom at the University of Pittsburgh for the XPS measurement. This work was performed at the JSNN, a member of Southeastern Nanotechnology Infrastructure Corridor (SENIC) and National Nanotechnology Coordinated Infrastructure (NNCI), which is supported by the National Science Foundation (ECCS-1542174).

References

1. Zhu, S.; Meng, Q.; Wang, L.; Zhang, J.; Song, Y.; Jin, H.; Zhang, K.; Sun, H.; Wang, H.; Yang, B. Highly Photoluminescent Carbon Dots for Multicolor Patterning, Sensors, and Bioimaging Angew. Chem., Int. Ed. **2013**, 52, 3953– 3957 DOI: 10.1002/anie.201300519

2. Lim, S. Y.; Shen, W.; Gao, Z. Carbon Quantum Dots and Their Applications Chem. Soc. Rev. **2015**, 44, 362– 381 DOI: 10.1039/C4CS00269E

3. Zheng, X. T.; Ananthanarayanan, A.; Luo, K. Q.; Chen, P. Glowing Graphene Quantum Dots and Carbon Dots: Properties, Syntheses, and Biological Applications Small **2015**, 11, 1620– 1636 DOI: 10.1002/smll.201402648

4. Liu, D.; Qu, F.; Zhao, X.; You, J. Generalized One-Pot Strategy Enabling Different Surface Functionalizations of Carbon Nanodots to Produce Dual Emissions in Alcohol–Water Binary Systems J. Phys. Chem. C **2015**, 119, 17979– 17987 DOI: 10.1021/acs.jpcc.5b05786

5. Wang, Y.; Hu, A. Carbon Quantum Dots: Synthesis, Properties and Applications J. Mater. Chem. C **2014**, 2, 6921– 6939 DOI: 10.1039/C4TC00988F

6. Li, X.; Rui, M.; Song, J.; Shen, Z.; Zeng, H. Carbon and Graphene Quantum Dots for Optoelectronic and Energy Devices: A Review Adv. Funct. Mater. **2015**, 25, 4929– 4947 DOI: 10.1002/adfm.201501250

7. Xu, Q.; Wei, J.; Wang, J.; Liu, Y.; Li, N.; Chen, Y.; Gao, C.; Zhang, W.; Sreeprased, T. S. Facile Synthesis of Copper Doped Carbon Dots and Their Application as a ″Turn-Off″ Fluorescent Probe in the Detection of Fe^{3+} Ions RSC Adv. **2016**, 6, 28745– 28750 DOI: 10.1039/C5RA27658F

8. Kumar, V. B.; Borenstein, A.; Markovsky, B.; Aurbach, D.; Gedanken, A.; Talianker, M.; Porat, Z. Activated Carbon Modified with Carbon Nanodots as Novel Electrode Material for Supercapacitors J. Phys. Chem. C **2016**, 120, 13406– 13413 DOI: 10.1021/acs.jpcc.6b04045

9. Jiang, H.; Chen, F.; Lagally, M. G.; Denes, F. S. New Strategy for Synthesis and Functionalization of Carbon Nanoparticles Langmuir **2010**, 26, 1991– 1995 DOI: 10.1021/la9022163

10. Xu, Z.-Q.; Lan, J.-Y.; Jin, J.-C.; Dong, P.; Jiang, F.-L.; Liu, Y. Highly Photoluminescent Nitrogen-Doped Carbon Nanodots and Their Protective Effects against Oxidative Stress on Cells ACS Appl. Mater. Interfaces **2015**, 7, 28346– 28352 DOI: 10.1021/acsami.5b08945

11. Das, B.; Dadhich, P.; Pal, P.; Srivas, P. K.; Bankoti, K.; Dhara, S. Carbon Nanodots from Date Molasses: New Nanolights for the *in Vitro* Scavenging of Reactive Oxygen Species J. Mater. Chem. B **2014**, 2, 6839– 6847 DOI: 10.1039/C4TB01020E

12. Sachdev, A.; Gopinath, P. Green Synthesis of Multifunctional Carbon Dots from Coriander Leaves and Their Potential Application as Antioxidants, Sensors and Bioimaging Agents Analyst **2015**, 140, 4260– 4269 DOI: 10.1039/C5AN00454C

13. Zhao, S.; Lan, M.; Zhu, X.; Xue, H.; Ng, T.-W.; Meng, X.; Lee, C.-S.; Wang, P.; Zhang, W. Green Synthesis of Bifunctional Fluorescent Carbon Dots from Garlic for Cellular Imaging and Free Radical Scavenging ACS Appl. Mater. Interfaces **2015**, 7, 17054– 17060 DOI: 10.1021/acsami.5b03228

14. Foti, M. C.; Daquino, C.; Geraci, C. Electron-Transfer Reaction of Cinnamic Acids and Their Methyl Esters with the DPPH$^{\bullet}$ Radical in Alcoholic Solutions J. Org. Chem. **2004**, 69, 2309– 2314 DOI: 10.1021/jo035758q

15. Jha, N. S.; Mishra, S.; Jha, S. K.; Surolia, A. Antioxidant Activity and Electrochemical Elucidation of the Enigmatic Redox Behavior of Curcumin and Its Structurally Modified Analogues Electrochim. Acta **2015**, 151, 574– 583 DOI: 10.1016/j.electacta.2014.11.026

16. Khoshtariya, D. E.; Dolidze, T. D.; Zusman, L. D.; Waldeck, D. H. Observation of the Turnover between the Solvent Friction (Overdamped) and Tunneling (Nonadiabatic) Charge-Transfer Mechanisms for A Au/$Fe(Cn)_6^{3-/4-}$ Electrode Process and Evidence for a Freezing out of the Marcus Barrier J. Phys. Chem. A **2001**, 105, 1818– 1829 DOI: 10.1021/jp0041095

17. Qu, S.; Wang, X.; Lu, Q.; Liu, X.; Wang, L. A Biocompatible Fluorescent Ink Based on Water-Soluble Luminescent Carbon Nanodots Angew. Chem., Int. Ed. **2012**, 51, 12215– 12218 DOI: 10.1002/anie.201206791

18. Garcia, E. J.; Oldoni, T. L. C.; Alencar, S. M. d.; Reis, A.; Loguercio, A. D.; Grande, R. H. M. Antioxidant Activity by DPPH Assay of Potential Solutions to Be Applied on Bleached Teeth Braz. Dent. J. **2012**, 23, 22– 27 DOI: 10.1590/S0103-64402012000100004

19. Cui, Q.; Xu, J.; Wang, X.; Li, L.; Antonietti, M.; Shalom, M. Phenyl-Modified Carbon Nitride Quantum Dots with Distinct Photoluminescence Behavior Angew. Chem., Int. Ed. **2016**, 55, 3672– 3676 DOI: 10.1002/anie.201511217

20. Lim, C. S.; Hola, K.; Ambrosi, A.; Zboril, R.; Pumera, M. Graphene and Carbon Quantum Dots Electrochemistry Electrochem. Commun. **2015**, 52, 75– 79 DOI: 10.1016/j.elecom.2015.01.023

21. Muthulingam, S.; Bae, K. B.; Khan, R.; Lee, I.-H.; Uthirakumar, P. Improved Daylight-Induced Photocatalytic Performance and Suppressed Photocorrosion of N-Doped ZnO Decorated with Carbon Quantum Dots RSC Adv. **2015**, 5, 46247– 46251 DOI: 10.1039/C5RA07811C

22. Hou, H.; Banks, C. E.; Jing, M.; Zhang, Y.; Ji, X. Carbon Quantum Dots and Their Derivative 3D Porous Carbon Frameworks for Sodium-Ion Batteries with Ultralong Cycle Life Adv. Mater. **2015**, 27, 7861– 7866 DOI: 10.1002/adma.201503816

23. Zhang, M.; Bai, L.; Shang, W.; Xie, W.; Ma, H.; Fu, Y.; Fang, D.; Sun, H.; Fan, L.; Han, M.Facile Synthesis of Water-Soluble, Highly Fluorescent Graphene Quantum Dots as a Robust Biological Label for Stem Cells J. Mater. Chem. **2012**, 22, 7461– 7467 DOI: 10.1039/c2jm16835a

24. Zhang, J.; Abbasi, F.; Claverie, J. An Efficient Templating Approach for the Synthesis of Redispersible Size-Controllable Carbon Quantum Dots from Graphitic Polymeric Micelles Chem. - Eur. J. **2015**, 21, 15142– 15147 DOI: 10.1002/chem.201502158

25. Feng, J.; Liu, G.; Yuan, S.; Ma, Y. Influence of Functional Groups on Water Splitting in Carbon Nanodot and Graphitic Carbon Nitride Composites: A Theoretical Mechanism Study Phys. Chem. Chem. Phys. **2017**, 19, 4997– 5003 DOI: 10.1039/C6CP08622E

26. Zeng, Z.; Zhang, W.; Arvapalli, D.; Bloom, B.; Sheardy, A.; Mabe, T.; Liu, Y.; Chevva, H.; Waldeck, D. H.; Wei, J.; Ji, Z. A Fluorescence-Electrochemical Study of Carbon Nanodots (CNDs) in Bio- and Photoelectronic Applications and Energy Gap Investigation Phys. Chem. Chem. Phys. **2017**, 19, 20101 DOI: 10.1039/C7CP02875J

27. Li, X.; Zhang, S.; Kulinich, S. A.; Liu, Y.; Zeng, H. Engineering Surface States of Carbon Dots to Achieve Controllable Luminescence for Solid-Luminescent Composites and Sensitive Be^{2+} Detection Sci. Rep. **2015**, 4, 4976 DOI: 10.1038/srep04976

28. Fu, M.; Ehrat, F.; Wang, Y.; Milowska, K. Z.; Reckmeier, C.; Rogach, A. L.; Stolarczyk, J. K.; Urban, A. S.; Feldmann, J. Carbon Dots: A Unique Fluorescent Cocktail of Polycyclic Aromatic Hydrocarbons Nano Lett. **2015**, 15, 6030– 6035 DOI: 10.1021/acs.nanolett.5b02215

29. Loukanov, A.; Sekiya, R.; Yoshikawa, M.; Kobayashi, N.; Moriyasu, Y.; Nakabayashi, S. Photosensitizer-Conjugated Ultrasmall Carbon Nanodots as Multifunctional Fluorescent Probes for Bioimaging J. Phys. Chem. C **2016**, 120, 15867– 15874 DOI: 10.1021/acs.jpcc.5b11721

30. Zhu, H.; Wang, X.; Li, Y.; Wang, Z.; Yang, F.; Yang, X. Microwave Synthesis of Fluorescent Carbon Nanoparticles with Electrochemiluminescence Properties Chem. Commun. **2009**, 5118– 5120 DOI: 10.1039/b907612c

31. Bukman, L.; Martins, A. C.; Barizão, É. O.; Visentainer, J. V.; Almeida, V. d. C. DPPH Assay Adapted to the FIA System for the Determination of the Antioxidant Capacity of Wines: Optimization of the Conditions Using the Response Surface Methodology Food Anal. Methods **2013**, 6, 1424– 1432 DOI: 10.1007/s12161-012-9560-x

32. Solon, E.; Bard, A. J. The Electrochemistry of Diphenylpicrylhydrazyl J. Am. Chem. Soc. **1964**, 86, 1926– 1928 DOI: 10.1021/ja01064a005

33. Taylor, A. W.; Puttick, S.; Licence, P. Probing Solvation in Ionic Liquids via the Electrochemistry of the DPPH Radical J. Am. Chem. Soc. **2012**, 134, 15636– 15639 DOI: 10.1021/ja3052816

34. Andrei, V.; Bunea, A.-I.; Tudorache, A.; Gáspár, S.; Vasilescu, A. Simple DPPH.-Based Electrochemical Assay for the Evaluation of the Antioxidant Capacity: A Thorough Comparison with Spectrophotometric Assays and Evaluation with Real-World Samples Electroanalysis **2014**, 26, 2677– 2685 DOI: 10.1002/elan.201400376

35. Ahmed, S.; Tabassum, S.; Shakeel, F.; Khan, A. Y. A Facile Electrochemical Analysis to Determine Antioxidant Activity of Flavonoids against DPPH Radical J. Electrochem. Soc. **2012**, 159, F103– F109 DOI: 10.1149/2.jes112300

36. Bhatti, N. K.; Subhani, M. S.; Khan, A. Y.; Qureshi, R.; Rahman, A. Heterogeneous Electron Transfer Rate Constants of Viologen Monocations at a Platinum Disk Electrode Turk. J. Chem. **2006**, 30, 165– 180

37. Muhammad, H.; Tahiri, I. A.; Muhammad, M.; Masood, Z.; Versiani, M. A.; Khaliq, O.; Latif, M.; Hanif, M. A Comprehensive Heterogeneous Electron Transfer Rate Constant Evaluation of Dissolved Oxygen in DMSO at Glassy Carbon Electrode Measured by Different Electrochemical Methods J. Electroanal. Chem. **2016**, 775, 157– 162 DOI: 10.1016/j.jelechem.2016.05.049

38. Scharifker, B. R. Diffusion to Ensembles of Microelectrodes J. Electroanal. Chem. Interfacial Electrochem. **1988**, 240, 61– 76 DOI: 10.1016/0022-0728(88)80313-9

39. Abdullah, S.; Kamarudin, S. K.; Hasran, U. A.; Masdar, M. S.; Daud, W. R. W. Electrochemical Kinetic and Mass Transfer Model for Direct Ethanol Alkaline Fuel Cell (DEAFC) J. Power Sources **2016**, 320, 111– 119 DOI: 10.1016/j.jpowsour.2016.04.003

40. Paradas, M.; Campaña, A. G.; Jiménez, T.; Robles, R.; Oltra, J. E.; Buñuel, E.; Justicia, J.; Cárdenas, D. J.; Cuerva, J. M. Understanding the Exceptional Hydrogen-Atom Donor Characteristics of Water in Ti^{III}-Mediated Free-Radical Chemistry J. Am. Chem. Soc. **2010**, 132, 12748– 12756 DOI: 10.1021/ja105670h